JOURNAL OF COMPUTATIONAL PHYSICS 78, 64–78 1988

A Numerical Method for the Incompressible Navier–Stokes Equations in Three-Dimensional Cylindrical Geometry*

JOHN C. STRIKWERDA† AND YVONNE M. NAGEL

Mathematics Research Center, University of Wisconsin-Madison, Madison, Wisconsin 53705

Received August 5, 1986; revised July 23, 1987

We describe a numerical method for solving the steady, three-dimensional, incompressible Navier–Stokes equations in cylindrical geometry. Also, we present results of computations in which this method is used to determine the flow in fluid-filled cylinders undergoing spinning and coning motion. Second-order accurate central finite difference formulas are used to approximate derivatives in the radial and axial directions and a Fourier method is used to approximate the angular derivatives. Nonuniform grids are used to improve the resolution of the velocity and pressure near the cylinder walls. The system of difference equations is solved using an iterative method based on successive-over-relaxation. The method has been found to be very efficient in terms of both computer time and storage. Results of the numerical method applied to the flow in spinning and coning cylinders are presented for several cases for which experimental data are available. In addition, perturbation methods are used to study the data at small coning speeds and small coning angles. Numerical results of this no-coning limit are compared with both the numerical data and experimental data at low coning conditions.

INTRODUCTION

We present a numerical method for solving the steady, incompressible Navier–Stokes equations in three-dimensional cylindrical geometry. The difference scheme is a regularized central difference scheme in the radial and axial direction as introduced by Strikwerda [17] with a Fourier method in the azimuthal direction. The method is presented as applied to the computation of the flow in a fluid-filled cylinder undergoing both a spinning and coning motion. The values of the velocity components and pressure are assigned to a common grid, i.e., a non-staggered grid is used, and grid stretching is used to improve the resolution near the cylinder walls. Because of the regularized difference method, the scheme maintains second-order accuracy even for nonuniform grids. The difference equations are solved by an iterative method based on successive-over-relaxation as discussed by Strikwerda

* Sponsored by the United States Army under Contract DAAG29-8-C-0041.
† Supported in part by National Science Foundation Grant MCS-8306880.

0021-9991/88 $3.00

[18] and thus requires only one three-dimensional array per dependent variable. This offers a significant savings in computer storage over time-marching methods. The iterative method uses lines successive-over-relaxation together with an exact inversion of the Fourier operator for each line. Each line consists of the points at a fixed value of the radial and axial coordinates.

The study of the flow in fluid-filled spinning cylinders is of importance in several areas, especially ballistics. Stewartson [16] studied the inviscid flow in a spinning cylinder and Wedemeyer [21, 22] applied this theory, along with some approximations, to the case of high Reynolds number flows. The low Reynolds number case is also of interest since projectiles filled with highly viscous fluids have exhibited rapid despin and growth in coning angle. In an effort to understand this phenomenon Miller [8, 9] and D'Amico and coworkers [12] devised experiments in which fluid-filled cylinders were subjected to simultaneous spinning and coning motions. Various researchers have made analytical studies of the problem, e.g., Herbert [6, 7] and Murphy [10, 11]. A numerical study was done using a finite difference, time-marching scheme by Vaughn, Oberkamps, and Wolfe [20] using a method of Chorin [2]. The present method was applied to this problem because of the need for a more efficient and accurate computer code for studying this fluid dynamics problem.

The paper is organized as follows. Section 1 describes the derivation of the equations to be solved by the numerical method. Section 2 presents the finite difference equations and the Fourier method for the incompressible Navier-Stokes equations. The iterative solution algorithm for the difference equations is discussed in Section 3. A perturbation expansion in terms of two small parameters is discussed in Section 4 and in Section 5 computational results are presented.

1. The Equations

Consider a fluid-filled cylinder which is spinning simultaneously about two axes. The first axis is that of the cylinder and the second axis, the coning axis, is inclined to the cylinder axis by a fixed angle θ. Let ω be the angular velocity with which the cylinder rotates about the coning axis and let Ω be the angular velocity of rotation about the cylinder axis. The fluid velocity, $\mathbf{v}$ and pressure, P, in the cylinder are governed by the incompressible Navier–Stokes equations given by

$$\begin{aligned} D\mathbf{v} &= -\nabla P + R^{-1}\nabla^2\mathbf{v} \\ \nabla\cdot\mathbf{v} &= 0, \end{aligned} \tag{1.1}$$

in an inertial frame in which the coning axis is fixed. The equations and variables are non-dimensionalized by using the cylinder radius, a, as the length scale and the product of the cylinder radius and the spin rate of the cylinder about its axis as the reference velocity, hence the Reynolds number is $\Omega a^2/\nu$, where ν is the kinematic

viscosity of the fluid. By changing to the non-inertial coordinate frame which rotates with angular velocity ω about the coning axis the fluid motion becomes steady. It is also convenient to compute the difference between the velocity and the solid body motion of the cylinder rather than the velocity itself. Similarly, it is convenient to compute with the difference between the pressure and a given function that is chosen to simplify the forcing terms arising from the coordinate transformations. This transformation was introduced by Vaughn *et al.* [20].

Based on these transformations, and using a cylindrical coordinate system aligned with the cylinder, the equations describing the flow are

$$-R^{-1}\nabla^2\mathbf{u} + (\mathbf{u}\cdot\nabla)\,\mathbf{u} + \frac{\partial \mathbf{u}}{\partial \phi} - \boldsymbol{\omega}(\tau, \theta)\times\mathbf{u} + \nabla p = 2\tau \sin\theta r\cos\phi\mathbf{k} \tag{1.2}$$

$$\nabla\cdot\mathbf{u} = 0, \tag{1.3}$$

where τ is the ratio of the angular velocity about the coning axis to that about the cylinder axis, i.e., ω/Ω, and $\mathbf{k}$ is the unit vector in the direction of the z axis, the cylinder axis, and

$$\begin{aligned}\boldsymbol{\omega}(\tau, \theta) &= 2(-\tau\sin\theta\cos\phi, \tau\sin\theta\sin\phi, 1+\tau\cos\theta)' \\ &= 2(1+\tau\cos\theta)\,\mathbf{k} - 2\tau\sin\theta\mathbf{i}(\phi)\end{aligned}$$

in the cylindrical coordinate system, where $\mathbf{i}(\phi)$ is the unit vector in the x direction. The $x-z$ plane is the plane of the two axes which is also the plane $\phi = 0$. The velocity $\mathbf{u}$ in Eqs. (1.2) and (1.3) is relative to the solid body rotation of the cylinder and in the coordinate system rotating with the coning motion, thus the boundary condition for the system (1.2), (1.3) is

$$\mathbf{u} = \mathbf{0} \tag{1.4}$$

on the cylinder boundary. The relations between the actual velocity and pressure $(\mathbf{v}, P)$ in Eq. (1.1) and the computed velocity and pressure $(\mathbf{u}, p)$ in Eqs. (1.2) and (1.3) are

$$\mathbf{u} = \mathbf{v} - \mathbf{k}\times\mathbf{r} - \boldsymbol{\tau}\times\mathbf{r} \tag{1.5}$$

$$p = P - \frac{1}{2}r^2 - r^2\tau\cos\theta - \frac{\tau^2}{2}((r\cos\phi\cos\theta + z\sin\theta)^2 + r^2\sin^2\phi), \tag{1.6}$$

where $\boldsymbol{\tau}$ is the vector in the direction of the coning axis with magnitude τ. The system (1.2), (1.3) holds for $0 \leqslant r \leqslant 1$ and $-b \leqslant z \leqslant b$, where b is the aspect ratio of the cylinder, defined by the ratio of the length of the cylinder to its diameter.

In addition to the system (1.2), (1.3), it is also of interest to examine the equations resulting from a linearization about τ and θ equal to zero, as will be discussed in Section 5. The resulting system is

$$-R^{-1}\nabla^2\mathbf{u} + \frac{\partial \mathbf{u}}{\partial \phi} - 2\mathbf{k}\times\mathbf{u} + \nabla p = 2r\cos\phi\mathbf{k} \tag{1.7}$$

$$\nabla\cdot\mathbf{u} = 0. \tag{1.8}$$

This system will also be used to explain the iterative solution algorithm which uses a linearization to determine the updates to the solution.

The choice of the reference velocity used here is the same as that used by Herbert [6, 7] and Vaughn *et al.* [20], however, it differs from that used in the experimental studies by Hepner [5], Nusca *et al.* [12], and in the analytical work of Murphy [10, 11]. In these works the reference angular velocity is $\Omega + \omega \cos\theta$, the angular velocity in the inertial frame. The nondimensional quantities using this experimental reference angular velocity will be distinguished with an asterisk as a superscript. The relationships between the Reynolds numbers and the relative coning velocities are given by

$$R^* = R(1 + \tau \cos\theta)$$

$$\tau^* = \frac{\omega}{\Omega + \tau \cos\theta} \tag{1.9}$$

$$= \frac{\tau}{1 + \tau \cos\theta}.$$

Notice that

$$1 + \tau \cos\theta = \frac{1}{1 - \tau^* \cos\theta}$$

and

$$\tau = \frac{\tau^*}{1 - \tau^* \cos\theta}.$$

2. The Numerical Method

The numerical method to solve the equations of flow is based on the regularized finite difference method of Strikwerda [17] together with a Fourier or pseudo-spectral method. Finite differences are used to approximate derivatives in the axial and radial direction and the Fourier method is used to approximate derivatives in the azimuthal direction. The Fourier method is much more accurate than the finite difference method for periodic independent variables such as ϕ (Gottlieb and Orszag, [4]), and this allows for a substantial savings in computer storage and thus also in computer run time. The regularized differences make it possible to compute both the velocity and pressure on the same grid, as opposed to staggered grid methods. Also, grid stretching is used to place more points in the regions near the container walls to better resolve the flow field. The rgularized differences allow this to be done simply without loss of accuracy. The nonuniform grid is defined with the use of mappings.

$$r = \alpha\rho + (1 - \alpha)\,\rho^3 \tag{2.1}$$

$$z = b(\beta\zeta + (1 - \beta)(15\zeta^3 - 8\zeta^5)/7), \tag{2.2}$$

which map the region $0 \leqslant \rho \leqslant 1$ and $-1 \leqslant \zeta \leqslant 1$ onto the cylinder. Because the resolution at the end walls was critical to the accuracy of the solution the stretching (2.2) was chosen to have the property that $d^2z/d\zeta^2$ vanishes at ζ equal to ± 1 so as to obtain a more uniform stretching there. The values of α and β are chosen to make $dr/d\rho$ and $dz/d\zeta$ less than 1 and b, respectively, at ρ and ζ equal to 1. The variables ρ, ζ, and the angular variable, ϕ, are discretized using uniform grid spacing, i.e.,

$$\begin{aligned} \Delta\rho &= 1/(I-1), & \rho_i &= (i-1)\,\Delta\rho, \\ \Delta\zeta &= 2/(K-1), & \zeta_k &= (k-1)\,\Delta\zeta, \\ \Delta\phi &= 2\pi/J, & \phi_j &= (j-1)\,\Delta\phi. \end{aligned}$$

The differential equations were written in terms of the new independent variables ρ and ζ and then differenced using central difference formulas. As an example,

$$\begin{aligned} \frac{1}{r}\frac{\partial}{\partial r}\left(r\frac{\partial u}{\partial r}\right) &= \frac{1}{rr'(\rho)}\frac{\partial}{\partial \rho}\left(\frac{r}{r'(\rho)}\frac{\partial u}{\partial \rho}\right) \\ &\approx \frac{1}{r_i r_i'}\left(\frac{r_{i+1/2}}{r'_{i+1/2}}u_{i+1,j,k}-u_{i,j,k}\right)-\frac{r_{i-1/2}}{r'_{i-1/2}}\left(u_{i,j,k}-u_{i-1,j,k}\right)\frac{1}{\Delta\rho^2}, \end{aligned} \tag{2.3}$$

where $r_i = r(\rho_i)$, $r'(\rho_i)$, etc. The gradient terms and the divergnce terms were differenced using regularized differences as introduced by Strikwerda [17]. For example, $\partial p/\partial z$ in (1.2) and $\partial u/\partial r$ in (1.3) were approximated by

$$\begin{aligned} \frac{\partial p}{\partial z_{i,j,k}} &\approx \frac{1}{z'(\zeta_k)}\left(\frac{p_{i,j,k+1}-p_{i,j,k-1}}{2\,\Delta\zeta}\right. \\ &\qquad \left.-\frac{p_{i,j,k+2}-3p_{i,j,k+1}+3p_{i,j,k}-p_{i,j,k-1}}{6\,\Delta\zeta}\right) \\ \frac{\partial ru}{r\partial r_{i,j,k}} &\approx \frac{1}{rr'(\rho_i)}\left(\frac{r_{i+1}u_{i+1,j,k}-r_{i-1}u_{i-1,j,k}}{2\,\Delta\rho}\right) \\ &\qquad -\frac{u_{i+1,j,k}-3u_{i,j,k}+3u_{i-1,j,k}-u_{i-2,j,k}}{6r'(\rho_i)\,\Delta\rho}. \end{aligned}$$

As discussed in Strikwerda [17], these regularized differences were used only on the terms $\partial p/\partial r$ and $\partial p/\partial z$ in the pressure gradient and on the terms $\partial ru/r\partial r$ and $\partial w/\partial z$ in the divergence equation. The approximations to $\partial p/\partial\phi$ and $\partial v/\partial\phi$ will be discussed later.

In the Fourier method approximations to derivatives with respect to the angular variable, ϕ, are obtained as follows, using the pressure as an example. For each

choice of the radial and axial grid indices, i and k, the discrete function $p_{i,j,k}$ is presented using the discrete Fourier transform as

$$p_{i,j,k} = \sum_{n=0}^{J/2}{}' a^{(4)}_{i,n,k} \sin n\phi_j + b^{(4)}_{i,n,k} \cos n\phi_j, \tag{2.4}$$

where $a^{(4)}_{i,0,k}$ and $a^{(4)}_{i,J/2,k}$ are 0, and the prime on the summation indicates that the first and last terms are weighted with a $\frac{1}{2}$. Similar expressions with coefficients $a^{(l)}_{i,n,k}$, $b^{(l)}_{i,n,k}$ hold for the velocity components u, v, and w, for $l = 1, 2, 3$, respectively. Considering the right-hand side of (2.4) as a continuous function of ϕ, and then differentiating this function with respect to ϕ we obtain

$$\frac{\partial p}{\partial \phi_{i,j,k}} \approx \sum_{n=0}^{J/2}{}' n a^{(4)}_{i,n,k} \cos n\phi_j - n b^{(4)}_{i,n,k} \sin n\phi_j. \tag{2.5}$$

The coefficients $a^{(4)}_{i,n,k}$ and $b^{(4)}_{i,n,k}$ are easily obtained by the use of formulas

$$a^{(4)}_{i,n,k} = \frac{2}{J} \sum_{j=0}^{J-1} p_{i,j,k} \sin n\phi_j$$

and

$$b^{(4)}_{i,n,k} = \frac{2}{J} \sum_{j=0}^{J-1} p_{i,j,k} \cos n\phi_j.$$

To maintain the regularity of the difference method (see Bube and Strikwerda [1]), the approximations to $\partial p/\partial \phi$ in the pressure gradient in (1.2) and $\partial v/\partial \phi$ in the divergence equation (1.3) were approximated as in (2.5) with the addition of the term

$$\tfrac{1}{8} b^{(4)}_{i,J/2,k} (-1)^j n \tag{2.6.}$$

to (2.5) and the subtraction of a similar term to compute $\partial v/\partial \phi$. The use of the factor $\frac{1}{8}$ was somewhat arbitrary, however the omission of this term (2.6) led to nonconvergence of the solution in almost all cases. The importance of such a term can be seen in that, without the term (2.6), the Fourier mode $b_{i,J/2,k} \cos \phi_j$ which is

$$b_{i,J/2,k} (-1)^j$$

will not contribute to the derivative (2.5). Thus the scheme would allow grid scale oscillations in the ϕ direction. The use of this extra term in occurrences of first derivatives of the velocity components with respect to ϕ in (1.2) or (1.7) resulted in poorer performance of the iterative solution algorithm and so was not used. The effect of the regularizing terms has to do only with removing high frequency oscillations and does not affect the formal accuracy of the method.

Along the z axis of the cylindrical coordinate system the values of the velocity and pressure were determined by interpolation from the neighboring grid points. In particular,

$$w_{1,j,k} = (4\bar{w}_{2,k} - \bar{w}_{3,k})/3$$

and

$$p_{1,j,k} = (4\bar{p}_{2,k} - \bar{p}_{3,k})/3,$$

where

$$\bar{w}_{i,k} = \frac{1}{J}\sum_{j=1}^{J} w_{i,j,k}$$

and similarly for $\bar{p}_{i,k}$. Note that $w_{1,j,k}$ and $p_{1,j,k}$ are independent of j. Because of the multiple-valued representation of the velocity along the axis of the cylindrical coordinate system we have

$$u_{1,j,k} = U_{1,k}\cos\phi_j + V_{1,k}\sin\phi_j$$
$$v_{1,j,k} = -U_{1,k}\sin\phi_j + V_{1,k}\cos\phi_j,$$

where $U_{1,k}$ and $V_{1,k}$ are the velocity components on the axis in the cartesian coordinate system. The values of $U_{1,k}$ and $V_{1,k}$ are given by

$$U_{1,k} = (4\bar{U}_{2,k} - \bar{U}_{3,k})/3$$
$$V_{1,k} = (4\bar{V}_{2,k} - \bar{V}_{3,k})/3$$

with

$$\bar{U}_{i,k} = \frac{1}{J}\sum_{j=1}^{J} u_{i,j,k}\cos\phi_j - v_{i,j,k}\sin\phi_j$$

and

$$\bar{V}_{i,k} = \frac{1}{J}\sum_{j=1}^{J} u_{i,j,k}\sin\phi_j + v_{i,j,k}\cos\phi_j.$$

As shown in Strikwerda and Nagel [19] this treatment at the origin preserves the second-order accuracy of the method.

The values of the pressure on the cylinder walls were determined by extrapolation from the interior by the formulas

$$p_{I,j,k} = 3p_{I-1,j,k} - 3p_{I-2,j,k} + p_{I-3,j,k}$$

and

$$p_{i,j,K} = 3p_{i,j,K-1} - 3p_{i,j,K-2} + p_{i,j,K-3}$$

and similarly for $p_{i,j,1}$.

3. The Iterative Solution Algorithm

The system of nonlinear difference equations is solved using a modified line successive-over-relaxation method (LSOR). The basic method is described in Strikwerda [18] for the case with linear finite difference equations. Because the Fourier method is used in the azimuthal direction it is most convenient to use line SOR, with each line being the grid points in the azimuthal direction for each given value of the radial and axial coordinates. The coupling between the three velocity components and the natural periodicity of the azimuthal coordinate leads to a periodic system of equations.

To describe the solution algorithm it is best to regard the discrete solution

$$(u_{i,j,k}, v_{i,j,k}, w_{i,j,k}, p_{i,j,k})$$

as continuous functions of ϕ with a finite Fourier expansion, that is, as

$$(u_{i,k}(\phi), v_{i,k}(\phi), w_{i,k}(\phi), p_{i,k}(\phi)) = (\mathbf{u}_{i,k}(\phi), p_{i,k}(\phi)).$$

The finite difference and Fourier scheme for the linearized problem (1.7) can be written as

$$\begin{aligned} &A^{i,k}_{i-1,k}\mathbf{u}_{i-1,k} + A^{i,k}_{i+1,k}\mathbf{u}_{i+1,k} + + A^{i,k}_{i,k-1}\mathbf{u}_{i,k-1} + A^{i,k}_{i,k+1}\mathbf{u}_{i,k+1} + A^{i,k}_{i,k}\mathbf{u}_{i,k} \\ &\quad + G_{i+2,k}\, p_{i+2,k} + G_{i+1,k}\, p_{i+1} + G^{i,k}_{i-1,k}\, p_{i-1,k} + G^{i,k}_{i,k+2}\, p_{i,k+2} \\ &\quad + G^{i,k}_{i,k+1}\, p_{i,k+1} + G^{i,k}_{i,k-1}\, p_{i,k-1} + G^{i,k}_{i,k}\, p_{i,k} = 2r_i \cos\phi_j \mathbf{k}, \end{aligned} \tag{3.1}$$

where each of $A^{i,k}_{i,k}$ and $G^{i,k}_{i,k}$ are matrices of differential operators in ϕ. In particular, the operator $A^{i,k}_{i,k}$ is

$$\begin{pmatrix} -R^{-1}\left(L_{i,k} + \dfrac{1}{r_i^2}\right) - \dfrac{\partial}{\partial\phi} & -R^{-1}\dfrac{2}{r_i^2}\dfrac{\partial}{\partial\phi} - 2 & 0 \\ -R^{-1}\dfrac{2}{r_i^2}\dfrac{\partial}{\partial\phi} + 2 & -R^{-1}\left(L_{i,k} + \dfrac{1}{r^2}\right) + \dfrac{\partial}{\partial\phi} & 0 \\ 0 & 0 & -R^{-1}L_{i,k} + \dfrac{\partial}{\partial\phi} \end{pmatrix}$$

where $L_{i,k}$ is the operator

$$\frac{1}{r_i r'_i}\left(\frac{r_{i+1/2}}{r'_{i+1/2}} + \frac{r_{i-1/2}}{r'_{i-1/2}}\right)\frac{1}{\Delta\rho^2} - \frac{1}{z'_k}\left(\frac{1}{z'_{k+1/2}} + \frac{1}{z'_{k-1/2}}\right)\frac{1}{\Delta\zeta^2} + \frac{1}{r_i^2}\frac{\partial^2}{\partial\phi^2}.$$

The iterative method is then written as

$$A^{i,k}_{i,k}(\mathbf{u}^{\nu+1}_{i,k} - \mathbf{u}^{\nu}_{i,k}) = \omega \mathbf{res}_{i,k} \tag{3.2}$$

where $\mathbf{res}_{i,k}$ is the difference of the right-hand and the left-hand sides of Eq. (3.1) evaluated using the most current values of $\mathbf{u}$, and ω is the SOR iteration parameter. Equation (3.2) was solved by computing the Fourier coefficients of the components of the velocity residual vector $\mathbf{res}_{i,k}$ for the current value of (i, k) and solving for the Fourier coefficients of the velocity update $\mathbf{u}_{i,k}^{\nu+1} - \mathbf{u}_{i,k}^{\nu}$. This leads to a set of linear equations for the Fourier coefficients of the velocity update which are solved by Gaussian elimination. Each linear system is of size at most six by six for the sine and cosine terms for each value of n as in (2.4) for the three components of the velocity update.

For the nonlinear system of equations the same algorithm was used with $\mathbf{res}_{i,k}$ being computed with the addition of the nonlinear convection terms.

After the velocity was updated at all the grid points by one pass of the LSOR operator, the pressure was updated by setting

$$p_{i,j,k}^{\nu+1} = p_{i,j,k}^{\nu} - \gamma \nabla_h \cdot \mathbf{u}_{i,j,k}^{\nu+1}, \tag{3.3}$$

where γ is an iteration parameter as described in Strikwerda [18] and $\nabla_h \cdot$ is the discrete divergence operator. As in Strikwerda [15, 16], we did not attempt to satisfy the equation

$$\nabla_h \cdot \mathbf{u}_{i,j,k} = 0, \tag{3.4}$$

but rather

$$\nabla_h \cdot \mathbf{u}_{i,j,k} = \delta_h, \tag{3.5}$$

where δ_h is the average value of the discrete velocity divergence. In all the cases presented here the value of δ_h was on the order of the truncation error. Since the method is second-order accurate (Strikwerda [17]) the error reflected in the δ_h should be consistent with the truncation error of the other equations and the actual calculations confirm this.

As discussed in Strikwerda [17], the difference equation (3.4) with the boundary conditions (1.4) will, in general, be an over-specified system and need not have a solution. By allowing the divergence of the velocity field to be a constant, but non-zero value, the system has a unique solution. This difficulty arises because there is no simple discrete analog of the divergence theorem for the grids employed in this work. A necessary condition for the differential divergence equation (1.8) to be satisfied is that the integral of the normal component of the velocity around the boundary vanish. This condition is certainly satisfied if the velocity is zero on the boundary. However, it is not clear what the necessary condition is for the discrete divergence equation (3.4) to be satisfied. Moreover, it is evident from numerical experiments that this necessary condition need not be satisfied even when the velocity vanishes at all boundaries. That is, there need be no solution to the discrete equations if one uses (3.4) rather than (3.5). However, there should be solutions that agree with (3.4) to within the overall truncation error and by employing (3.5) we obtain such a solution.

This method has the advantage that only one three-dimensional array is needed for each of the velocity and pressure variables as opposed to time-arching methods which require two such arrays. The LSOR iteration has a good rate of convergence, allowing for the solutions to be computed on a VAX 11/780 computer in at most several hours of cpu time. Most runs took much less than one hour of cpu time.

4. Perturbation Expansions in the Coning Speed and Angle

Many of the experimental results are for small values of the parameters τ and θ, therefore it is useful to make a perturbation expansion of the solution of the system (1.2) and (1.3) in terms of these parameters. Since the forcing term is proportional to $\tau \sin\theta$ the velocity and pressure are also proportional to this quantity. Consider then the expansion in the form

$$(\mathbf{u}, p) = \tau \sin\theta \sum_{m,n=0}^{\infty} (\mathbf{u}^{m,n}, p^{m,n})\, \tau^m \sin^n \theta. \tag{4.1}$$

For each term of the expansion we have

$$\nabla \cdot \mathbf{u}^{n,m} = 0,$$

and each $\mathbf{u}^{n,m}$ vanishes on the boudary. The equation for $(\mathbf{u}^{0,0}, p^{0,0}) = (\mathbf{u}^0, p^0)$ is the same as (1.7)

$$-R^{-1}\nabla^2 \mathbf{u}^0 + \frac{\partial \mathbf{u}^0}{\partial \phi} - 2\mathbf{k} \times \mathbf{u}^0 + \nabla p^0 = 2r \cos\phi \mathbf{k}. \tag{4.2}$$

This equation has been analyzed by Gerber *et al.* [3] for the case of high Reynolds number using separation of variables and numerical methods. If we let the operator on left side of Eq. (4.2) be denoted by L and $W^{m,n} = (\mathbf{u}^{m,n}, p^{m,n})$, we obtain

$$LW^{1,0} = -2\mathbf{k} \times \mathbf{u}^0 \tag{4.3}$$

and

$$LW^{0,1} = 0;$$

hence $W^{0,1} = 0$.

Since the operator L is linear and the forcing term in (4.2) involves only the $k = 1$ Fourier mode we see that W^0 and $W^{1,0}$ contain only the $k = 1$ Fourier mode. Similarly for $W^{1,2}$ and $W^{2,0}$ which satisfy

$$LW^{1,2} = \mathbf{k} \times \mathbf{u}^0, \qquad LW^{2,0} = -2\mathbf{k} \times \mathbf{u}^{1,0}.$$

The equation for $W^{1,1}$ has a right-hand side involving a quadratic in $\mathbf{u}^0$ and the vector $\mathbf{i}(\phi)$ times $\mathbf{u}^0$, and thus $W^{1,1}$ contains only the Fourier modes for $k = 0$ and 2. Similarly, $W^{2,1}$ also has only these modes.

Similar to Nusca *et al.* [12] we define the coefficient of pressure, C_p, as

$$\max |p_1(r, z)|\, \theta^{-1}$$

for values of (r, z) on the end wall of spinning and coning cylinders, where $p_1(r, z)$ is the amplitude of the Fourier mode for $k = 1$. That is, $p_1(r, z)$ is determined by

$$p(r, \phi, z) = \sum_{k=0}^{\infty} p_k(r, z) \sin(k\phi + \varepsilon_k).$$

From the perturbation expansion in τ and $\sin\theta$, and considering also the solid body contribution to the true pressure, e.g., (1.6), we obtain

$$C_p(r, z) = \tau((p^0_{1,s}(r, z) + \tau p^{1,0}_{1,s}(r, z))^2 + (p^0_{1,c}(r, z) + \tau p^{1,0}_{1,c}(r, z) + \tau r z)^2)^{1/2} + O(\tau^2 \sin^2\theta, \tau^3), \tag{4.4}$$

where the subscripts of s and c refer to the coefficients of $\sin\phi$ and $\cos\phi$. Note that the terms for $\tau^2 \sin\theta$ arising from $W^{1,1}$ do not affect C_p since $W^{1,1}$ involves only the Fourier modes for $k = 0$ and 2. Also we set C_p to have the same sign as τ.

The coefficients in (4.4) are easily computable. The coefficients $p^0_{1,s}$ and $p^0_{1,c}$ are computed by solving Eqs. (4.2). The coefficients $p^{1,0}_{1,s}$ and $p^{1,0}_{1,c}$ can be obtained either by solving the system (4.3) or, as was done here, by solving the system

$$-R^{-1}\nabla^2 \mathbf{u}^0 + \frac{\partial \mathbf{u}^0}{\partial \phi} - 2(1+\tau)\, \mathbf{k} \times \mathbf{u}^0 + \nabla p^0 = 2r \cos\phi \mathbf{k}. \tag{4.5}$$

This system is obtained by performing an expansion of the solution in terms of $\sin\theta$ only, similar to the way (4.2) was obtained. The system (4.5) was solved for θ equal to 0.0 and for τ equal to both a small positive and a small negative value. Accurate estimates of $p^{1,0}_{1,s}$ and $p^{1,0}_{1,c}$ can then be obtained by computing the divided difference of the Fourier coefficients of the pressure on the endwall using both values of τ. The experimental coefficient of pressure, C_p^*, is related to C_p by

$$C_p^* = \frac{C_p}{(1+\tau\cos\theta)^2} = C_p(1-\tau^*\cos\theta)^2,$$

similar to the relations (1.9).

The coefficients of liquid roll moment, C_{lrm}, and the coefficient of liquid side moment, C_{lsm}, see Murphy [10, 11], can also be developed as expansions in τ and $\sin\theta$ using the expansion (4.1). The expansions for C_{lrm} and C_{lsm} are

$$C_{\mathrm{lrm}} = \tau T_z^{1,1}(R, b)/2\pi b + O(\tau^2)$$

and

$$C_{\mathrm{lsm}} = T_x^{0,0}(R, b)/2\pi b + O(\tau),$$

where $T_z^{1,1}$ and $T_x^{0,0}$ are terms in the expansions of the moments of force resulting from (4.1). The yaw moment $T_x^{0,0}(R, b)$, and thus C_{lsm}^0, is easily obtained by solving the system (4.2). The despin moment $T_z^{1,1}$ is more difficult to obtain and no attempt was made to compute it.

5. Computational Results

The numerical method described above has been used to compute the flow in a spining and coning cylinder for a large number of cases. Here we present the result of a few repesentative runs. A discussion of other cases and their engineering significance will appear elsewhere.

Figure 1 displays the data for C_p^* measured on the endwall of the cylinder for the case $R^* = 3.1$, $b = 3.148$, and $\theta = 2°$. Fig. 1a shows $C_p^*(r, b)$ at the radial location $r = 0.667$ and Fig. 1b shows the same quantity at $r = 0.434$. The results of the computations are marked with a × and the gyroscope data of Hepner [5] are marked with a °. In addition to the data points, the curve giving C_p^* as a function of τ^* based on the expansion (4.4) for C_p is also displayed. Note that the computed solution and the curve based on (4.4) are not completely independent since the numerical method to compute the coefficients in (4.4) is essentially the same as the basic numerical method. Analytical results of Sedney [15] agree qualitatively with our computational results.

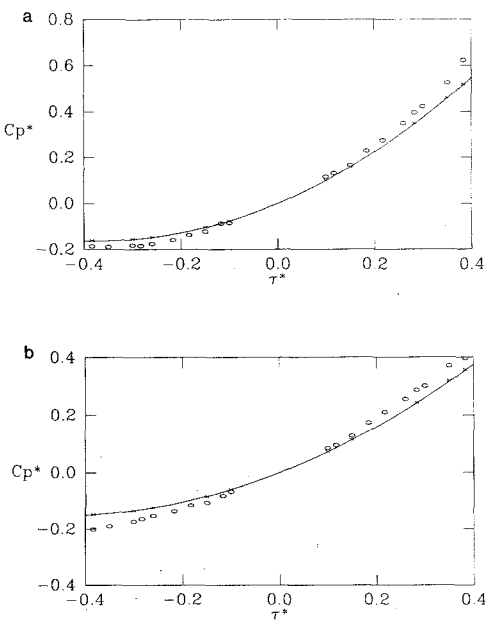

FIG. 1. (a) C_p^* vs τ^* at radius = 0.667; (b) C_p^* vs τ^* at radius = 0.434.

Figure 2 displays the coefficient of pressure C_p^* on the endwall as a function of radius for θ equal to 2° and two different values of τ^*. Figure 2a shows results for $\tau^* = 0.350$ and Fig. 2b displays results for $\tau^* = 0.100$, the experimental data and numerical results are marked as in Fig. 1. In both figures the excellent agreement between the basic numerical results and the perturbation results verifies the essential linearity of the problem for small values of τ and θ.

These calculations were made with $I = 11$, $J = 6$, $K = 33$, with grid stretching parameters α and β chosen so that the $dr/d\rho$ was 0.8 at $r = 1.0$ and $dz/d\zeta$ was $0.8b$ at $z = b$. The run with $\tau = 0.350$ took 82 iterations until the l^2 norm of the changes in each variable was less than 10^{-4}. This took approximately 550 s cpu time on the Vax 11/780 at the Mathematics Research Center.

Figure 3 displays C^0_{lsm} as a function of the Reynolds number, R, for the case $b = 2.20$ for R between 0 and 350. At τ equal to zero the side moment vanishes, nonetheless C^0_{lsm} need not vanish due to the scaling by τ in the definition of C_{lsm}. C^0_{lsm} is proportional to the derivative of the side moment with respect to τ at τ equal to zero. Since C_{lsm} is related to the yaw moment, a negative value of this quantity indicates a tendency to decrease the angular velocity about the coning axis and a positive value indicates a tendency to increase this angular velocity. The variation in the sign of C_{lsm} with increasing R is due to the reduction of the viscous effects on the moment as R is increased. Indeed, the contribution to C^0_{lsm} of the pressure on the side wall is of positive sign, the other contributions, i.e., pressure on the end wall and the viscous contribution, are all negative for this value of the aspect ratio.

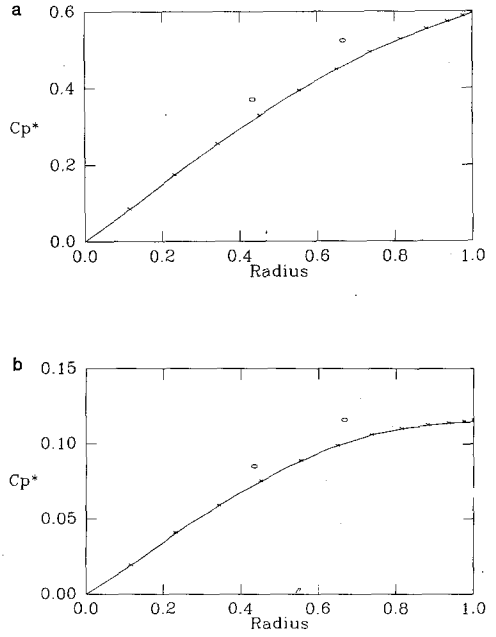

FIG. 2. (a) C_p^* vs radius at $\tau^* = 0.350$; (b) C_p^* vs radius at $\tau^* = 0.100$.

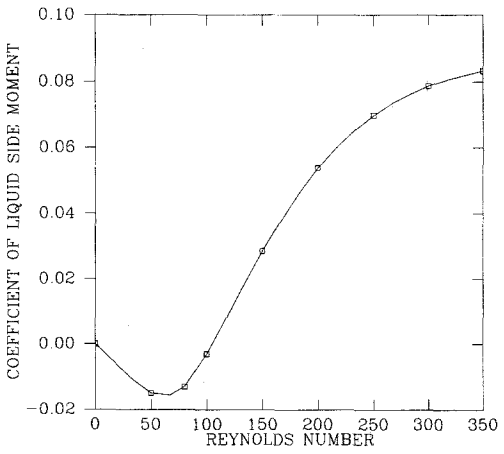

FIG.3. Coefficient of liquid side moment: ASP. = 2.200; $\tau = 0.000$.

As the Reynolds number increases the viscous side wall contribution decreases in magnitude changing the sign of C^0_{lsm}. A significant factor in the flight instability of liquid filled projectiles is an increase in the coning angular velocity and is most likely related to the positive values of C^0_{lsm} shown in Fig. 3. Notice that in the limit of τ equal to zero there is no distinction between R and R^*.

	$\theta = 2°$		Flight data		Computation	
R^*	τ^*	b	C_{lrm}	C_{lsm}	C_{lrm}	C_{lsm}
10.0	0.091	4.32	−0.025	0.020	−0.02375	0.02437
20.0	0.087	5.20	−0.040	0.040	−0.02984	0.03571
45.2	0.123	4.23	−0.055	0.050	−0.04454	0.04714

This table displays the moment values obtained by M. Nusca [13] using our code at Balistic Research Laboratory with experimental data obtained by R. L. Pope [14]. Values are given for both C_{lrm} and C_{lsm}. The code-generated moments agree with the experimental values to within the estimated experimental error.

6. CONCLUSIONS

The numerical method presented in this paper has been shown to be an efficient and accurate method for computing solutions to the steady incompressible Navoer–Stokes equations in three dimensions. The method has been applied to the computation of flows in cylinders undergoing spinning and coning motion and results agree well with experimental data. The use of the perturbation analysis corroborates the accuracy of the calculations.

ACKNOWLEDGMENTS

We wish to thank W. D'Amico, M. Mller, and M. Nusca for their assistance with the experimental data and their encouragement. We also thank the referees for their several comments.

REFERENCES

1. K. P. BUBE AND J. C. STRIKWERDA, *SIAM J. Numer. Anal.* **20**, 639 (1983).
2. A. J. CHORIN, *J. Comput. Phys.* **2**, 12 (1967).
3. N. GERBER, R. SEDNEY, AND J. M. BARTOS, ARBRL-TR-02422, October 1982 (unpublished).
4. D. GOTTLIEB AND S. A. ORSZAG, *Numerical Analysis of Spectral Methods: Theory and Applications* (SIAM, Philadelphia, 1977).
5. D. HEPNER, Experimental data, U.S. Army Ballistic Research Laboratory (unpublished).
6. T. HERBERT, CRDC-CR-84087, July 1984 (unpublished).
7. T. HERBERT, *J. Fluid Mech.* **167**, 181 (1986).
8. M. C. MILLER, CRDC-FP-84014, in *Proceedings of the 1983 Scientific Conference on Chemical Defense Research, October 1984.*
9. M. C. MILLER, *J. Guidance, Control, and Dynmics* **8**, 282 (1985).
10. C. H. MURPHY, AIAA-83-2142, August 1983 (unpublished).
11. C. H. MURPHY, *J. Guidance, Control, and Dynamics* **8**, 287 (1985).
12. M. J. NUSCA, W. P. D'AMICO, AND W. G. BEIMS, ARBRL-MR-03325, November 1983 (unpublished).
13. M. J. NUSCA AND W. P. D'AMICO, November 1983, Memorandum report in preparation (unpublished).
14. R. L. POPE, ARBRL-MR-03329, U.S. Army Ballistic Research Lab, Aberdeen Proving Ground, MD, Dec. 1983 (unpublished).
15. R. SEDNEY, private communication (1986).
16. K. STEWARTSON, *J. Fluid Mech.* **5** 577 (1959).
17. J. C. STRIKWERDA, *SIAM J. Sci. Statist. Comput.* **5**, 56 (1984).,
18. J. C. STRIKWERDA, *SIAM J. Numer. Anal.* **21**, 44 (1984).
19. J. C. STRIKWERDA AND Y. NAGEL, Math. Res. Center TSR 2934 (unpublished).
20. H. R. VAUGHN, W. L. OBERKAMPF, AND W. P. WOLFE, *J. Fluid Mech.* **150**, 121 (1985).
21. E. H. WEDEMEYER, BRL Report 1287, AD 472474, June 1965 (unpublished).
22. E. H. WEDEMEYER, BRL Report 1325, AD 48968, June 1966 (unpublished).